# Unveiling Year-Round Cropland Cover by Soil-Specific Spectral Unmixing of Landsat and Sentinel-2 Time Series

Felix Lobert [a, b, *], Marcel Schwieder [a, b], Jonas Alsleben [b], Tom Broeg [a], Katja Kowalski [c], Akpona Okujeni [b], Patrick Hostert [b, d], Stefan Erasmi [a]

[a] Thünen Earth Observation (ThEO), Thünen Institute of Farm Economics, Bundesallee 63, 38116 Braunschweig, Germany

[b] Earth Observation Lab, Geography Department, Humboldt-Universität zu Berlin, Unter den Linden 6, 10099 Berlin, Germany

[c] Earth Observation for Ecosystem Management, School of Life Sciences, Technical University of Munich, Hans-Carl-v.-Carlowitz-Platz 2, 85354 Freising, Germany

[d] Integrative Research Institute of Transformations of Human-Environment Systems (IRI THESys), Humboldt-Universität zu Berlin, Unter den Linden 6, 10099 Berlin, Germany

* Corresponding author.

E-mail address: felix.lobert@thuenen.de (F. Lobert).

*This paper is a non-peer-reviewed preprint submitted to EarthArXiv and is currently under review at Remote Sensing of Environment.*

## Abstract

Croplands are essential for food security but also impact the environment, biodiversity, and climate. Understanding, monitoring, modeling, and managing these impacts require accurate, comprehensive information on cropland vegetation cover.

This study aimed to continuously monitor the state and vegetative processes of cropland, focusing on the assessment of bare soil and its cover with photosynthetic vegetation (PV) and non-photosynthetic vegetation (NPV) at the national level. We employed regression-based unmixing techniques using time series of Sentinel-2 and Landsat imagery to quantify cover fractions of NPV, PV, and soil across the whole cultivation period. Our approach extends existing spectral unmixing methods by incorporating a novel soil-specific unmixing process based on a soil reflectance composite, which accounts for variations in the spectral characteristics of soils.

All cover fractions were predicted with mean absolute errors between 0.13 and 0.19. Introducing soil-specific unmixing improved the accuracy of soil and NPV fractions without compromising PV predictions, particularly benefiting areas with bright soils. These findings demonstrate the efficacy of our method in accurately predicting crop cover throughout the cultivation period and underline the added value of incorporating the soil adjustment into the unmixing workflow.

The contributions of this research are twofold: first, it provides essential data for the continuous monitoring of cropland cover, supporting agricultural carbon cycle and soil erosion modeling. Second, it enables further investigation into cropland management practices, such as cover cropping and tillage, through time series analysis techniques. This work underscores the potential of advanced spectral unmixing methods for enhancing agricultural monitoring and management strategies.

**Keywords**

agriculture; monitoring; vegetation; fractional cover; NPV

**Highlights**

- Spatially explicit soil-specific unmixing of Sentinel-2 and Landsat time series
- Unique bare soil spectrum identified for each pixel from soil reflectance composite
- Support Vector Regression models trained on synthetic spectral libraries
- Soil-specific predictions improved for NPV and soil, not impaired for PV
- Soil accuracy improvements did not compromise NPV, and vice versa

## 1. Introduction

Approximately a quarter of the European Union's (EU) land is covered by cropland making it the second largest land cover type in the EU after woodlands (Eurostat, 2024). While being the foundation of food security, croplands can also have significant negative environmental, biodiversity, and climate impacts (Dudley and Alexander, 2017; Kross et al., 2022). Among the effects are greenhouse gas (GHG) emissions, soil erosion, nitrogen leakage, and habitat loss. However, the net impact of these effects is not always negative and largely depends on management practices and use intensity (Lal, 2009; Poeplau and Don, 2015; Tscharntke et al., 2012).

Continuous cover of agricultural soils is an essential management practice for addressing several environmental issues. The sequestration of carbon in the soil, effectively removing $CO_2$ from the atmosphere, is significantly enhanced when fields are, e.g., continuously cultivated with cover crops instead of leaving fields as bare fallow (Johnson et al., 2007; Lal, 2009; Poeplau and Don, 2015). Reducing bare soil periods also mitigates soil erosion by maintaining the soil structure (Cerdan et al., 2010; Panagos et al., 2015). Additionally, it can prevent nitrogen leakage into ground- and surface water, thereby protecting water quality and promoting sustainable agricultural practices (Hively et al., 2020). To accurately assess the overall impact of cropping on the environment, comprehensive information on cropland cover is essential, and improved data quality can help reduce uncertainties in the modeling of soil factors and processes such as carbon dynamics (McClelland et al., 2021; Öttl et al., 2024; Seitz et al., 2023).

Earth observation (EO) enables frequent, broad-scale monitoring of cropland and has proven effective for tasks such as producing annual crop type maps (Blickensdörfer et al., 2022; Pham et al., 2024), delineating agricultural parcels (Tetteh et al., 2023), or analyzing crop phenology (Bolton et al., 2020; Lobert et al., 2023). Some studies also directly focused on monitoring specific cropland management practices. Among them are the detection of cover crops (Schulz et al., 2021), the identification of bare soil (Mzid et al., 2021), and the assessment of soil erosion (Vrieling, 2006). While providing valuable information, most products are static snapshots, lacking the ability to map nuanced variations in crop dynamics and growing periods (McClelland et al., 2021). Binary classification products can furthermore oversimplify cropland cover characterization as they do not capture land cover dynamics and neglect, e.g., states other than bare soil or cover crops, such as mulch, spontaneous vegetation, or volunteer grain. A generic and versatile concept of describing the dynamics of agricultural land cover with EO data is the analysis of fractional cover time series (Kowalski et al., 2022; Lewińska et al., 2020). Within this concept, the spectral signal captured by the satellite sensor is modeled as a mixture of defined endmembers according to their ground cover fractions. Unmixing spectral signals into cover fractions has a long history in satellite remote sensing. Starting from spectral mixture analysis (SMA) through area-weighted linear combinations of endmember spectra (Adams et al., 1986) or its variants such as Multiple Endmember Spectral Mixture Analysis (MESMA; Roberts et al., 1998), recent approaches make use of regression-based unmixing (Atkinson et al., 1997; Carpenter et al., 1999). Here, ML models estimate the cover fractions based on prior training using quantitative samples, which consist of mixed spectra labeled with their corresponding mixing fractions. To overcome the challenge of scarce training data, regression-based unmixing using synthetic training data generated from endmember spectra (Okujeni et al., 2013) provides a robust solution.

On agricultural land, the three main cover fractions are photosynthetic vegetation (PV), non-photosynthetic vegetation (NPV), and bare soil. The time series of these fractional cover estimates provide quantitative and interpretable units and were shown to support the investigation of environmental and management impacts on agricultural land (Guerschman et al., 2020). Among them are the mapping of crop residues (Barnes et al., 2021), short-term vegetation loss (Lewińska et al., 2020), and soil properties (Bouroubi et al., 2014). However, existing unmixing studies for agricultural land often cover limited study areas (Coulibaly et al., 2021; Yue et al., 2020) or only short periods (Li et al., 2016; Meusburger et al., 2010; Pacheco and McNairn, 2010), while wall-to-wall cover and high resolution long-term fractional cover time series are needed to support monitoring tasks and the evaluation of agricultural policies. Okujeni et al. (2024) demonstrated that the PV, NPV, and soil fractional cover time series retrieval method for grasslands, initially proposed for Sentinel-2 data by Kowalski et al. (2023), is both transferable to the Landsat archive and applicable on a national scale in Germany. This method's adaptability to multiple satellite sensors provides two significant advantages for large-scale monitoring activities. First, utilizing all available Sentinel-2 and Landsat observations maximizes potential revisit times (Lewińska et al., 2024), which is particularly important in regions with frequent cloud cover, such as the winter season in Germany (Mzid et al., 2021). Second, this allows to go back in time prior to the Sentinel era facilitating multidecadal monitoring applications.

In contrast to grassland, where moments of pure bare soil states are rare (Okujeni et al., 2024), we are faced with significantly more and longer bare soil periods in cropland. The wide variety of soils and factors influencing soil reflectance, like, soil type and moisture, lead to distinct spectral signatures and can cause confusion between NPV and PV when dealing with spectral unmixing (Guerschman et al., 2015; Yue et al., 2020, 2019). Yue et al. (2019) examined this issue in detail and proposed a dynamic soil endmember selection based on soil moisture. The method resulted in an improvement of their rice residue cover estimations on four test fields in China with the same soil type. However, spatially and temporally accurate information on soil moisture and other soil parameters are required, which are not always available at the desired resolution. Furthermore, they added that soil moisture only influences the soil spectrum to a certain extent and that the spectrum also depends on the soil color, organic carbon content, and texture. Although their approach represented a valuable initial step in addressing the issue, further research is necessary to account for the variability of soils in spectral unmixing.

The overall goal of this study is the development of an approach for continuously monitoring the cropland cover with NPV and PV for large areas, by adapting a regression-based unmixing method originally developed for estimating fractional cover time series of grassland (Kowalski et al., 2023; Okujeni et al., 2024) utilizing all available Sentinel-2 and Landsat 8/9 imagery in Germany for 2011-2023. We extended the method by developing unmixing models specific to different soil reflectance groups that we identified from a soil reflectance composite of Germany following Broeg et al. (2024). With this, we address the challenge of a large variety of factors that affect soil reflectance (Yue et al., 2019) and the often high spectral similarity of soil and NPV in multispectral data, depending on soil color, organic carbon content, and texture (Verrelst et al., 2023).

We aim to answer the following research questions:

1. How accurately can we estimate the fractional cover of PV, NPV, and soil for cropland with regression-based unmixing of harmonized Sentinel-2 and Landsat imagery?
2. How much does incorporating soil reflectance groups in the unmixing approach improve the results?
3. How do multi-year time series of fractional cover predictions vary depending on different cropland cover conditions throughout the season?

## 2. Study Area and Data

### *2.1. Study area*

The research was conducted across Germany, which spans approximately 357,592 km². Around half of this area is utilized for agricultural purposes, which splits up into roughly 70% cropland and 30% permanent grassland (Federal Statistical Office, 2024). The country's landscape is diverse, featuring the flat North German Plain, the undulating Central Uplands, and the mountainous regions of the Alps in the south.

Germany's soils accordingly also vary widely, including highly productive loess soils in the central and eastern regions, sandy soils in the North, and clayey/loamy soils in the southern areas. The country also encompasses multiple climate zones: the northern and northwestern parts experience a maritime climate with mild temperatures and moderate to high rainfall, influenced by the North Sea and the Baltic Sea. The eastern and southeastern regions have a continental climate, marked by hot summers and cold winters. Central Germany exhibits a transitional climate that combines elements of both maritime and continental climates, offering moderate temperatures and variable precipitation. The Alpine region in the south is characterized by cooler conditions, higher precipitation, and frequent snowfall, leading to shorter growing seasons (Deutscher Wetterdienst, 2024).

*2.2. Remote Sensing Imagery*

We used an available datacube of harmonized Sentinel-2 and Landsat 8/9 for Germany, comprising all scenes with cloud cover below 75%. Landsat data were acquired as Level-1TP, while Sentinel-2 data was obtained as Level-1C. The scenes were pre-processed and corrected for radiometric and geometric effects using the Level 2 processing system of the Framework for Operational Radiometric Correction for Environmental Monitoring (FORCE; Frantz, 2019). All data were projected and resampled to a common grid with a pixel size of 10 m. For Landsat imagery, nearest neighbor resampling was used. All data were then stored in the FORCE data cube structure consisting of non-overlapping 30 x 30 km tiles, creating an analysis-ready dataset (ARD).

We further improved the spectral consistency across the sensors in our datacube by adjusting the reflectance values of all Landsat sensors and bands to the corresponding reflectance values of Sentinel-2 using slopes and intercepts from a reduced major axis regression derived by Okujeni et al. (2024). Bands for atmospheric correction, panchromatic and thermal bands, and bands not common to all sensors used were not further considered. This resulted in 6 bands covering the blue, green, red, near-infrared (NIR), and shortwave-infrared (SWIR 1 and 2) wavelengths.

*2.3. Reference Data*

*Aerial Imagery*

We derived fractional cover reference data from a very high resolution (VHR; 30 cm) aerial imagery mosaic for Germany (acquired between 2019 and 2022) provided by the German Federal Agency for Cartography and Geodesy (BKG). Following the approach proposed by Kowalski et al. (2023), we sampled Sentinel-2 pixels on croplands in Germany, where cloud-free Sentinel-2 observations were available with less than five days deviation from the acquisition date of the aerial image at that specific point. The sampling was stratified by the dominating crop types in Germany: winter wheat, winter barley, winter rye, rapeseed, silage and grain maize, spring barley, oat, and potato which were taken from annual German-wide crop type maps (Blickensdörfer et al., 2022; Schwieder et al., 2024). Furthermore, we ensured that a variety of different fraction mixtures were included by equalized random sampling observations from bins with 0.2 step size based on the Normalized Difference Vegetation Index (NDVI; Tucker, 1979) and the SWIR ratio ($\rho SWIR1$ / $\rho SWIR2$; see Kowalski et al., 2022). For each sampled 10 m pixel, a grid of 100 sub-pixels of 1 m was constructed to assist the labeling process. By visually interpreting the VHR imagery, the dominant cover fraction (NPV, PV, or soil) was assigned to each sub-pixel.

Subsequently, the fractional covers for each 10 m pixel were calculated through aggregation. We removed samples located on field edges to other land use types like streets, residential areas, or hedges. Our sampling design resulted in 201 labeled Sentinel-2 pixels distributed across Germany's croplands (Fig. 1A). The different acquisition dates of the VHR mosaic furthermore led to coverage of data from multiple years and seasons (Fig. 1B/C).

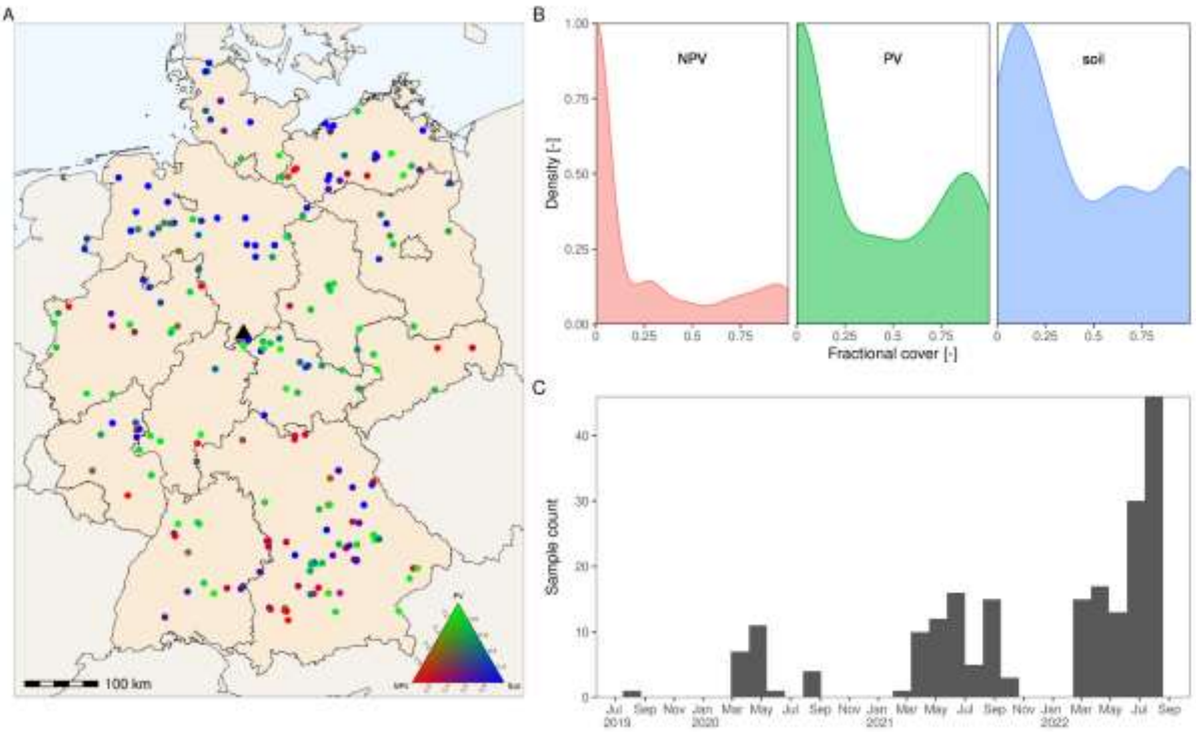


*Figure 1. Locations of the labeled Sentinel-2 pixels colored by their labeled cover fractions (A; the black triangle marks the area for which field observations were available), distribution of labeled fractional covers (A), and temporal distribution of the samples (B).*

*Field Observations*

We additionally had access to data from a field survey that was carried out between July 2023 and May 2024. During this period, cropland fields near the city of Göttingen in Lower Saxony (Fig. 1A) were visited repeatedly. The observation frequency ranged from up to weekly visits during phases of rapid plant growth and phenological development to bimonthly visits during the vegetative dormant phase in winter. Photos of the field cover were taken during each visit. Next to the cover photos, we had access to field boundaries and main crop types, and, if present, cover crop types were known for the observed fields.

## 3. Methods

We employed regression-based unmixing using synthetic training data from spectral libraries (Okujeni et al., 2017, 2013). Specifically, we adapted the generalized workflow for fractional cover time series retrieval for grasslands by Kowalski et al. (2023) and Okujeni et al. (2024) for monitoring croplands. We extended the approach to build unmixing models specific to different soil reflectance groups. This approach involves multiple steps that are explained in the following subsections:

1. creation of a soil reflectance composite for Germany and grouping of soils according to their spectral properties
2. compilation of a spectral library containing pure spectra, hereafter referred to as endmembers, representing NPV, PV, and soil for different crops and soil reflectance groups
3. synthetic mixing of the endmembers to create soil-specific training datasets for regression modeling
4. training of regression models and prediction of NPV, PV, and soil fractional cover time series based on Sentinel-2 and Landsat imagery
5. validation of the predicted fractional cover time series by a quantitative comparison with reference data derived from VHR imagery and a qualitative comparison with photos from field observations

### *3.1. Mapping Soil Reflectance Groups*

We divided the soils in Germany into different spectral groups to account for their spectral variability in our unmixing approach. This was based on a soil reflectance composite we derived following Broeg et al. (2024). We used all available Sentinel-2 and Landsat 8/9 imagery from our datacube between 2011 and 2023 and applied a dynamic threshold-based function using the NDVI and Normalized Burn Ratio 2 (NBR2; Van Deventer et al., 1997) to the time series of each pixel.

NDVI shows high values for PV and lower values for soil and NPV. While NDVI alone is not reliable for detecting bare soil (Demattê et al., 2018), NBR2 was shown suitable for separating bare and dry soils from wet soils and NPV (Dvorakova et al., 2023). We used the thresholds established by Broeg et al. (2024) for detecting bare soil in the context of soil organic carbon estimation and excluded observations with an NDVI above 0.45 or an NBR2 above 0.16. We discarded values greater than the 15$^{th}$ percentile of the remaining NBR2 values of each pixel to further minimize any non-bare soil influence. We then derived the soil reflectance composite by pixel-wise averaging all remaining observations.

We constructed soil reflectance groups by randomly sampling 250,000 points from the soil reflectance composite and applying the K-means algorithm (Lloyd, 1982). Based on iterative testing, we found that using six groups provided the best balance between capturing the variability in soil reflectance and maintaining meaningful distinctions between different soil types. Consequently, we assigned every pixel of the soil reflectance composite to its nearest soil reflectance group centroid, ensuring that each pixel was classified according to the most representative soil reflectance signature within our predefined groups.

### *3.2. Spectral Library Compilation*

We developed an image spectral library using two different strategies, with PV and NPV endmembers obtained separately from soil endmembers. PV and NPV endmembers were based on the triangular feature space concept, wherein a triangular space spans along the two dimensions of SWIR ratio and NDVI, with endmember candidates positioned on the vertices of the space (Guerschman et al., 2009; Kowalski et al., 2022). We stratified our endmember selection along annual national crop type maps (2017 to 2019; Blickensdörfer et al., 2022) and created a comprehensive, multitemporal feature space by sampling 10,000 points per year and crop type to represent the heterogeneity of cropland cover in Germany. For each location, we extracted all Sentinel-2 observations of the respective years, to exploit the higher spatial resolution compared to Landsat, which increases the probability of identifying pure spectra. After constructing an NDVI/SWIR ratio feature space for each crop, we identified candidate spectra by selecting the greenest pixels for PV, which corresponded to observations with the highest NDVI and lowest SWIR ratio values. For NPV, we chose the driest pixels, characterized by observations with the lowest NDVI and SWIR ratio values. We summarized all potentially pure PV and NPV spectra by calculating the 25$^{th}$, 50$^{th}$, and 75$^{th}$ percentile spectra to reduce computational costs while maintaining the class-wise spectral variability. A detailed description of this procedure can be found in Kowalski et al. (2023).

Soil endmembers were taken from the soil reflectance composite. The reflectance values were summarized to the 25$^{th}$, 50$^{th}$, and 75$^{th}$ percentiles for each soil reflectance group analogous to the PV and NPV spectra using the derived soil reflectance group map.

### *3.3. Synthetic Training Data Generation*

The compiled spectral library served as the foundation for creating synthetically mixed spectra and associated mixing proportions that were used as training data in the regression-based unmixing method. The approach for generating synthetic mixtures was originally introduced by Okujeni et al. (2013) and has been continuously enhanced. We followed the descriptions in Cooper et al. (2020) and Okujeni et al. (2021), which are based on a randomized mixing strategy to create separate sets of synthetic training data for each cover fraction of interest to train single-output regressors.

We created 1,000 synthetic mixtures for each cover fraction based on the spectral library. Each synthetic mixture comprised two to three endmembers from the three cover fractions randomly sampled from the library. These were then linearly combined with random fractions assigned to each endmember class, ensuring the fractions always sum up to 1. The resulting synthetic spectrum was then added to the training dataset, with the six spectral bands as input variables and the share of the target cover fraction as the label. Additionally, we included a shade spectrum in the synthetic mixtures to represent direct and structural shade components (Shimabukuro and Smith, 1991). The shade endmember, with a near-zero reflectance of 0.01 across all bands, was treated like any other endmember during the mixing step but was not considered as target fraction.

We created two different types of synthetic training datasets for each cover fraction to assess the influence of soil variety in the unmixing procedure:

1. Soil-specific synthetic training datasets: Separately for each soil reflectance group, considering only the soil endmembers from the same soil reflectance group to train soil-specific models.
2. Global synthetic training datasets: Considering all soil endmembers simultaneously to train a global model.

We replicated each training set generation five times. This enabled us to train an ensemble of regression models and aggregate the results afterward. This approach resulted in one global and six soil-specific training data compositions for each cover fraction and a total of 105 training datasets after replication.

### *3.4. Regression-Based Unmixing*

The training data sets were used to train global and soil-specific Support Vector Regression (SVR) models for the prediction of fractional cover time series based on Sentinel-2 and Landsat data. We used a grid search combined with 10-fold cross-validation to determine the optimal gamma and c parameters for each SVR model as model parameterization strategy following van der Linden et al. (2015). The trained models were applied to each image in our datacube which covered the reference data. The global model was applied to all pixels, while the soil-specific models were applied to pixels based on their grouping in the soil reflectance map. Predictions from the ensemble of models trained on the replicated training sets were averaged per pixel. The predicted values were normalized per pixel by dividing each fractional cover by the sum of the fractional cover. This ensured that the fractional covers always sum up to one. For the plots covered by the available field observation data, we subsequently summarized the predictions for all pixels within the field boundaries to the median for each observation. To mitigate edge effects, we applied a negative buffer of 20 m.

### *3.5. Validation*

We validated our predictions against the reference samples derived from VHR imagery (see section 2.3) based on the mean absolute error (MAE) and the coefficient of determination ($R^2$). The MAE gives an overview of the general error magnitude in the same unit as the predictions, while $R^2$ offers insight into how well the model predictions explain the variation in the reference data. These calculations were performed for each reference sample and its nearest corresponding prediction within a ±5-day window. Together, these metrics enabled us to compare the performance across different cover fractions and the global or soil-specific unmixing models. Following this quantitative evaluation, we plotted the time series for the plots covered by the available field observation data alongside a selection of cropland cover photos, enabling the visual interpretation of their correspondence with the actual cover observed in the field.

## 4. Results

### *4.1. Mapping Soil Reflectance Groups*

The soil reflectance composite reflects the overall diversity of soils in Germany (Fig. 2A). Dark soils, with higher organic carbon contents, are visible in central and Northwest Germany, while brighter sand-rich soils with low carbon contents are present in the Northeast and East. The results of the k-Means algorithm summarize these patterns into soil reflectance groups with similar spectral properties (Fig. 2B). Darker soils are categorized into groups 1 to 3, while the bright, yellowish soils belong to groups 5 and 6. Soils with medium brightness are found in group 4. The summarized spectral signatures of these groups built the basis for extracting the soil endmembers that were used for the soil spectral library compilation (Fig. 3). Here, next to the general brightness gradient across all bands, some differences could be observed. While most groups show a similar slope between SWIR1 and SWIR2, soil group 3 shows considerably less slope in this part of the spectrum. This is especially of interest since the spectra of the soil groups 2 and 3 are nearly identical in the visible and near but show high differences in the SWIR. We have also found differences in the red range that make the course from green to NIR either straight (groups 4 to 6) or with a bend (groups 1 to 3).

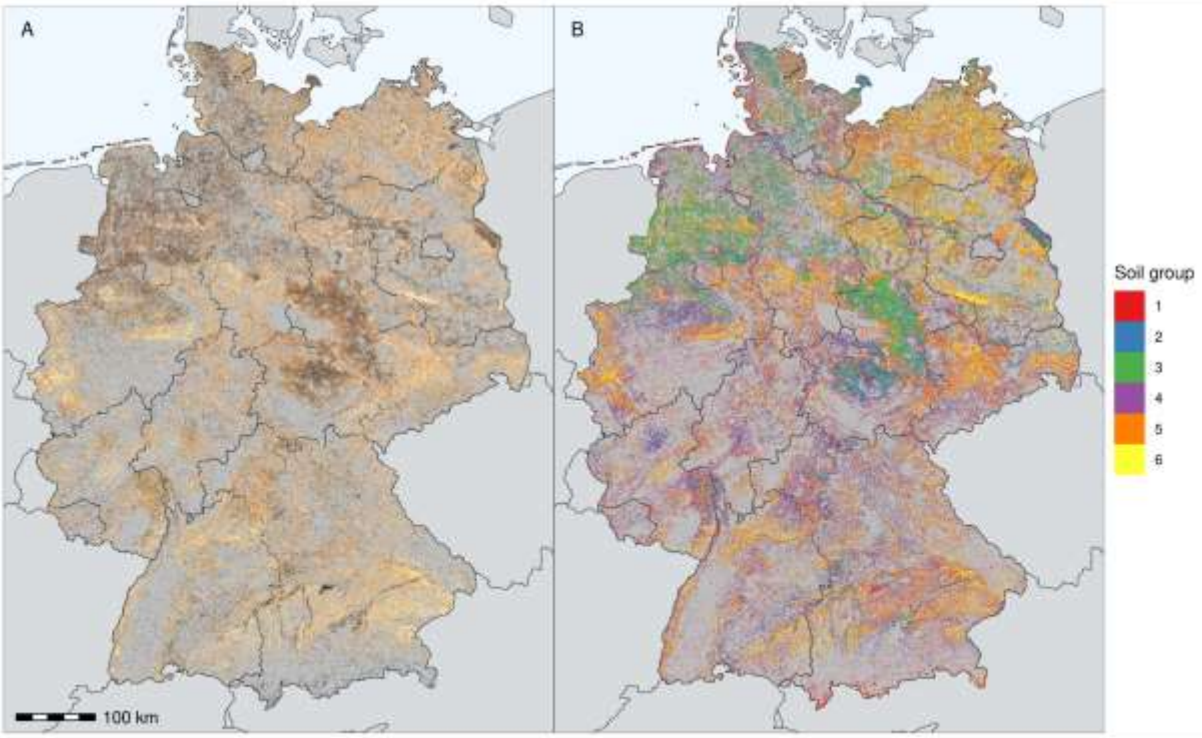


*Figure 2. Soil reflectance composite of German croplands in RGB true-color representation (A) and map of the derived soil reflectance groups (B).*

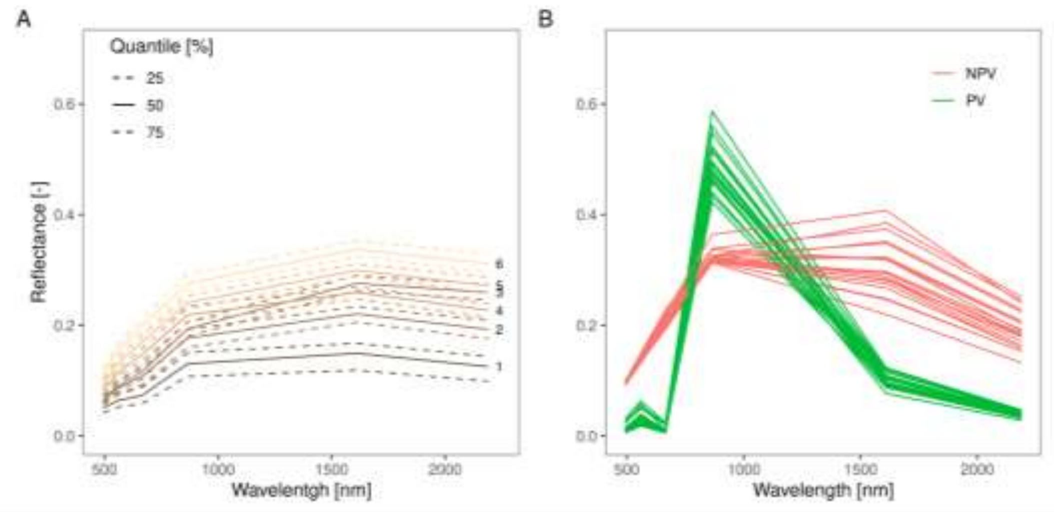


*Figure 3. Quantile spectra of extracted soil endmembers for different reflectance groups, with line colors representing the average RGB true color of each group (A), and spectra of PV and NPV endmembers across all crop types and quantiles included in the spectral library (B).*

### *4.2. Accuracy of Fractional Cover Predictions*

Scatterplots of reference data against predicted fractions offer a detailed insight into both modeling setups (Fig. 4). For the NPV fraction, both models reveal high scattering. We also observed a tendency to overestimate fractions near zero. Nevertheless, MAE and $R^2$ improved with the soil-specific model, indicating overall better estimates. For PV, both the global and soil-specific models produced similar results and showed the least scattering of all three cover fractions. While $R^2$ was identical for both models, MAE was only marginally impaired with the soil-specific model. Both models showed nearly identical point patterns, indicating consistent performance across both approaches. For the soil fraction, both models again show scattering, and an underestimation of values particularly close to 1. The soil fraction also benefited from the soil-specific modeling approach. The global model showed an MAE of 0.159, while the soil-specific model reduced the MAE to 0.141. The scatterplots confirmed this improvement, indicating better performance, particularly at higher soil fractions, which is shown by the regression line that is much closer to the 1:1 line.

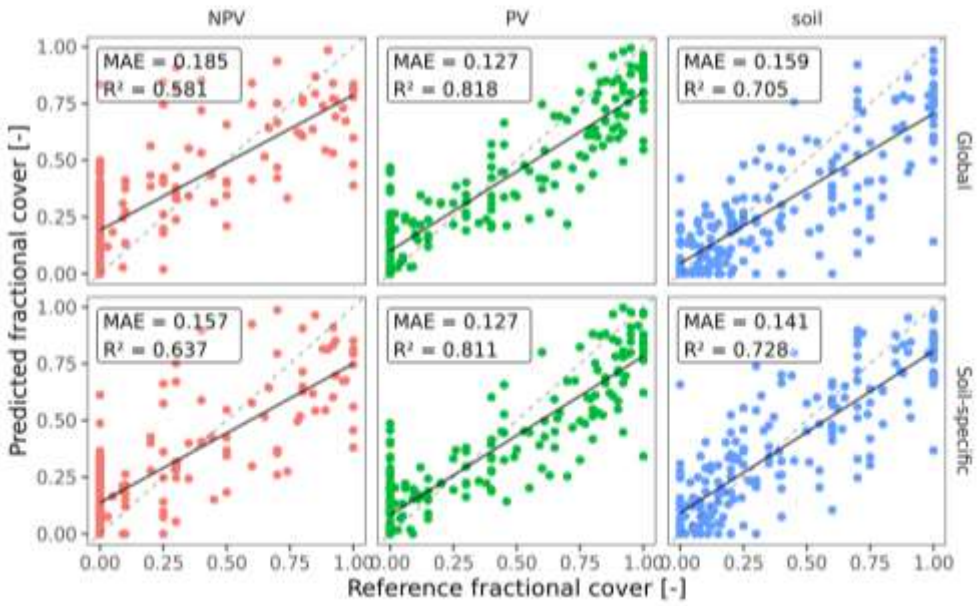


*Figure 4. Scatterplots of predicted and reference fractional covers with regression line (solid) and 1:1 line (dashed) for NPV, PV, and soil for the global (top) and soil-specific (bottom) models.*

The error metrics and improvements with soil-specific models varied across soil reflectance groups (Fig. 5). For NPV, the global model showed the highest errors in soil reflectance groups 4 and 5, with MAEs of 0.22 and 0.21. The soil-specific models improved the predictions for these groups, reducing the MAE by up to 0.04, while smaller reductions were seen in groups with generally lower errors in the global model, where MAEs ranged from 0.15 to 0.17. For PV, the global model's errors showed little variation across soil reflectance groups, with a slightly higher MAE in group 3. The soil-specific models had minimal impact on the PV fraction, with only a slight decrease in MAE for soil reflectance groups 3 and 5, where errors were already relatively low with the global model. For the soil fraction, the global model had the highest MAEs in groups 1 and 5, while group 6 had the lowest. The soil-specific models improved accuracy, particularly in groups 1 and 5, where the MAE decreased by up to 0.03, addressing the largest initial errors.

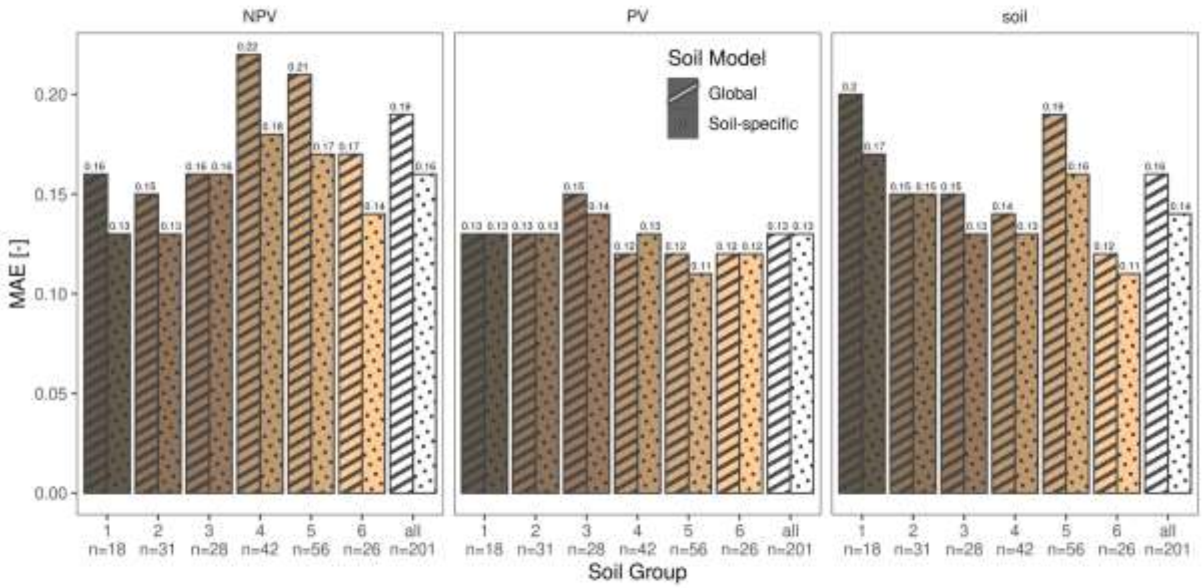


*Figure 5. Mean absolute error for the three cover fractions stratified by soil reflectance group for the global and soil-specific unmixing models. The fill color of the bars represents the average RGB true color of the respective soil reflectance group.*

When analyzing the soil fraction in more detail, we observed that the soil-specific model had varying impacts on the prediction accuracy across different soil reflectance groups. While for most soil reflectance groups the MAE decreased, observing the scatterplots revealed a more nuanced picture (Fig. 6). In the case of bright soils, there was a notable adjustment of the regression line towards the 1:1 line, particularly at higher soil fractions close to 1. This was reflected by a substantial increase in $R^2$ for groups 3 to 6. In contrast, predictions for dark soils (groups 1 and 2) exhibited a decrease in $R^2$, while a slight general upward shift of all values is visible.

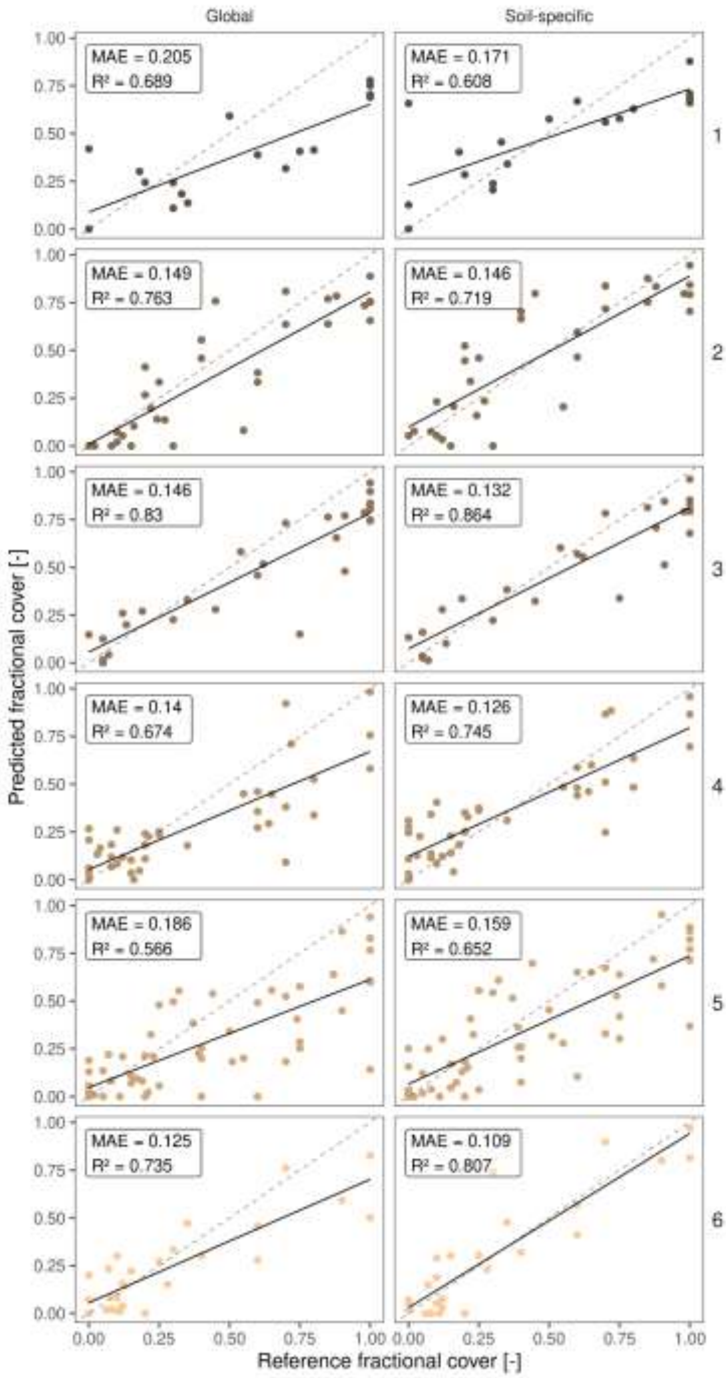


*Figure 6. Scatterplots between predicted and reference soil cover fractions stratified by soil reflectance group (rows) for the global and soil-specific unmixing models (dot colors refer to the average RGB true color of the respective soil reflectance group).*

## 4.3. *Fractional Cover Maps*

Spatial patterns of the predictions are illustrated for an exemplary area in Southern Germany in the federal state of Bavaria (Fig. 7). The false-color composite uses SWIR2 in the red channel, NIR in the green channel, and the red band in the blue channel and is scaled between the 3rd and 97th percentile per band. As a result, bare soil is represented by magenta tones due to its relatively high reflectance in both the SWIR2 and red bands, combined with lower reflectance in the NIR band. PV appears green because it reflects strongly in the NIR band while having lower reflectance in the SWIR2 and red bands. NPV is shown in blue because it has lower reflectance in the SWIR2 and NIR bands but higher reflectance in the red band, leading to a dominance of blue tones in the composite. The soil reflectance group map shows the variation in soil reflectance across this region. Darker soils (groups 1 to 3) dominate the southern regions, while brighter soils (groups 4 to 6) are more prevalent in the North and Northwest.

In the global model predictions, we observe frequent mixtures of NPV and soil (purple pixels) in the North and Northwest, alongside fields dominated by PV (green) and NPV (red). In the southern regions, fewer NPV-soil mixtures are present, with fields more commonly characterized by pure pixels of soil, PV, or NPV. This pattern aligns with the distribution of soil groups, where brighter soils (groups 4 to 6) tend to have more NPV-soil mixtures, while darker soils (groups 1 to 3) show more pure soil pixels.

In contrast, the soil-specific predictions produce a more consistent map. Fields in the North and Northwest that exhibited NPV-soil mixtures on pure soils in the fraction maps under the global model are now showing more realistic fractional covers that better match the false-color composite. Overall, the influence of soil reflectance groups on the predictions and spatial patterns of cover fractions is less pronounced in the soil-specific model, leading to a more uniform distribution across the area.

Another interesting finding is, that fields with high NPV fractions in the global predictions do not change in the soil-specific ones, while other areas, especially those with high soil fractions, exhibit an adjustment through the consideration of soil reflectance groups in the prediction. This matches our observations from Fig. 6, that especially high soil fractions on bright soils are underestimated with the global model, while the soil-specific models can account for that and predict high soil fractions on bright soils better.

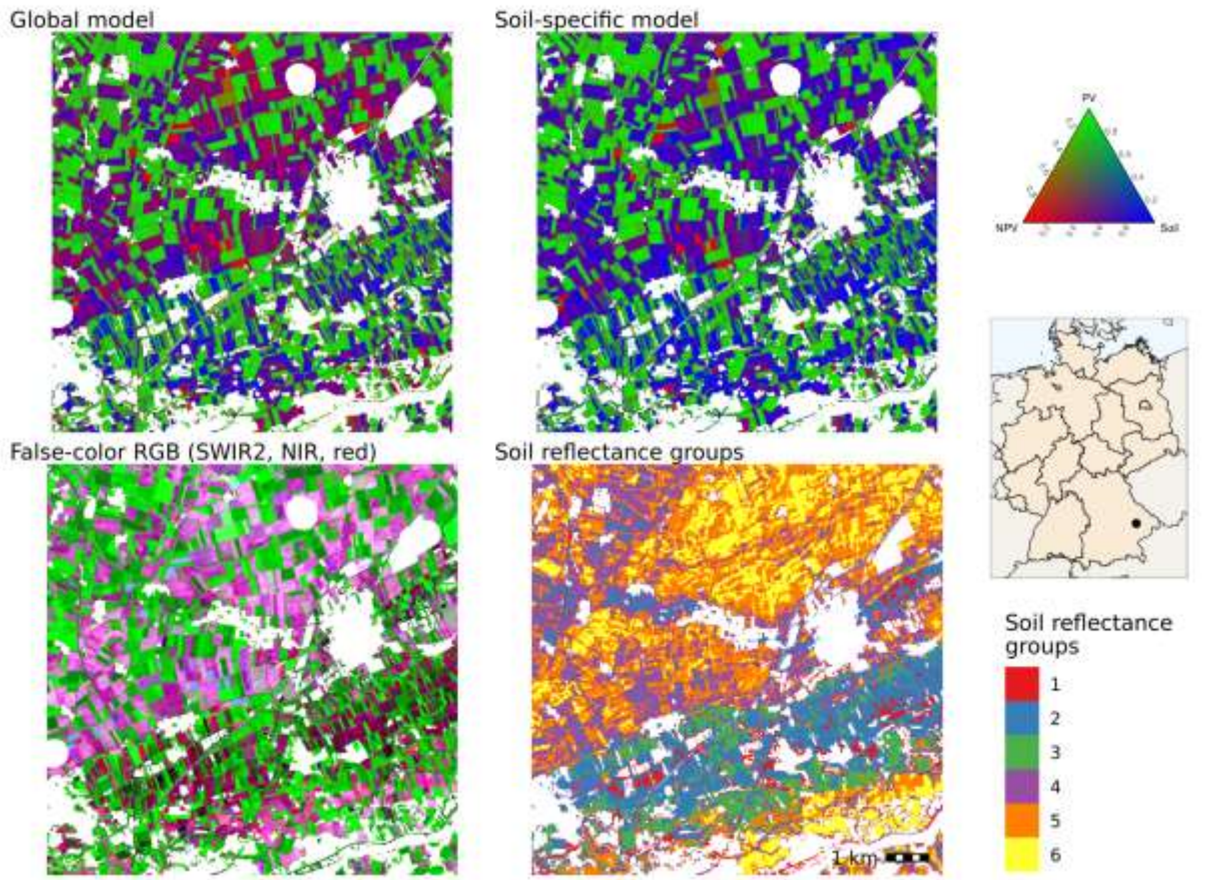


*Figure 7. Predictions from the global and soil-specific unmixing models and false-color composite based on a Sentinel-2 scene from May 28, 2023, together with the soil reflectance groups for a site in Bavaria.*

The zoom-ins in Fig. 8 enable a more detailed comparison of soil-specific and global modeling results along with coincident orthophotos across four landscape subsets and for different phases of the growing season. Panels A and B illustrate landscapes with small to medium-sized agricultural fields after the growing season for winter crops and at the beginning of ripening for summer crops. The harvested cropland is characterized by tillage activities leading to diverse patterns of bare fields with varying amounts of crop residues. Both the global and soil-specific models effectively capture the spatial variability evident in the orthophotos, particularly in distinguishing between areas of bare soil and vegetation. When comparing the soil-specific with the global predictions, we observe higher shares of NPV mixtures with soils predicted by the global model. In contrast, the higher soil cover depictable in the aerial photos is also represented by higher soil fractions in the unmixing results. This is consistent with the patterns seen in Fig. 7. Panel C shows a site with larger fields during stem elongation of winter crops and seedbed preparation for summer crops, where fields are predominantly covered by PV and soil. Here, notable intra-field differences are distinctly visible, demonstrating the models' sensitivity in distinguishing different cover fractions even on a fine scale. There are no noticeable differences between the global and soil-specific predictions. Panel D features a site with smaller fields towards or after harvest for winter crops and during the vegetative phase for summer crops. Fully matured winter crops show high NPV fractions and fields with summer crops are fully covered by PV. Both models capture the borders and differences between the fields, even in areas that have been partially harvested. The only notable difference is the higher soil share predicted by the soil-specific model. Notably, fields with high NPV fractions are not reduced in the soil-specific predictions, underscoring that soil-specific modeling does not simply result in reduced NPV predictions.

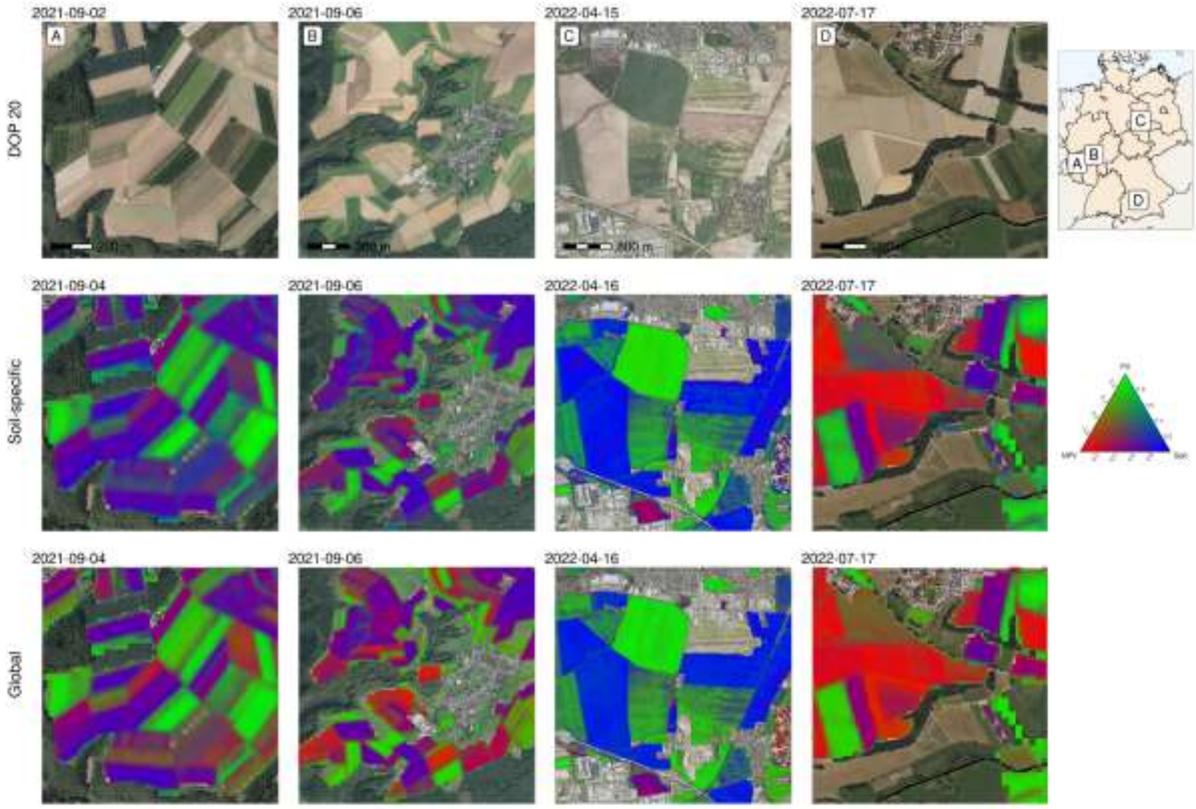


*Figure 8. Orthophotos (20 cm; © GeoBasis-DE / BKG [2024]) and corresponding cover fraction estimates from global and soil-specific models based on the closest Sentinel-2 observation for different sites in Germany.*

*4.4. Evaluating Fractional Cover Time Series*

The computation of fractional cover maps for the plots covered by the field observation data based on the available Sentinel-2 and Landsat images enabled the generation and qualitative analysis of fractional cover time series. Figures 9 and 10 show examples of such time series for different soil reflectance groups and two-year crop sequences.

Fig. 9 shows a field belonging to soil reflectance group 6 initially cultivated with winter wheat in 2023, followed by a cover crop during winter and the seeding of a summer crop in spring 2024. At the beginning of June, the field exhibited nearly full PV cover, with minimal soil and NPV presence. This was followed by a rapid decline in PV and a corresponding increase in NPV. This also becomes visible from image A in mid-July, where the winter wheat had reached full yellow ripeness. Up to this point, the time series are very similar to those in Fig. A.2.

Following tillage at the end of August, the green-up of a cover crop was visible in September, as shown in image D. This quickly reduced the estimated share of bare soil. The measured increase in NPV during this time does seem counterintuitive and appears to be an overestimate. By November, field visits confirmed the cover crop had fully grown, as seen in images E and F. Starting in December, the NPV share began to increase, reaching a maximum of over 0.8 by the end of January, which is caused by the dying off of the cover crop. During this period, the estimated share of PV steadily decreased, hitting a minimum in February. This transition is evident in images G and H, which show only residues of the cover crop and bare soil being left from mid-February on. The estimated soil share also began to rise, slightly lagging behind the changes in NPV, and reached a maximum of nearly full cover by May. This increase corresponds with images I and J, which reveal mulch tillage and the sowing of a summer crop.

Differences between global and soil-specific modeling become more evident here, compared to Fig. 10. Especially in May where nearly full soil cover is visible from the field observations, the global model predicts around 30% NPV and only 70% soil, while the soil-specific model corrects these values to less than 10% NPV and 90% soil. Major differences between both models are also visible during September 2023 and January 2024.

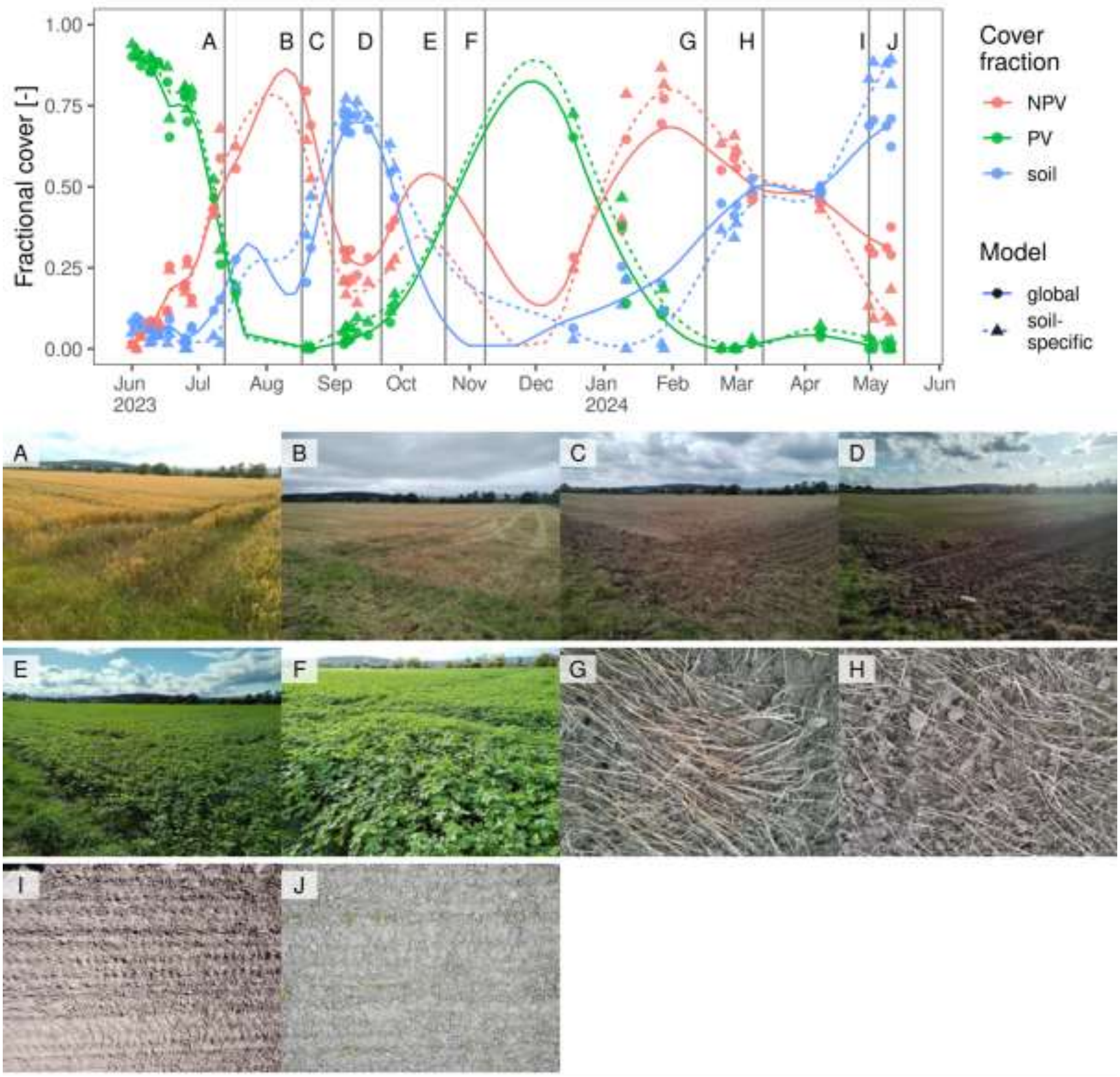


*Figure 9. Predicted fractional cover time series for photosynthetic vegetation (PV), non-photosynthetic vegetation (NPV), and soil for a field initially cultivated with winter wheat in 2023, followed by a cover crop during winter and the seeding of a summer crop in spring, supplemented with photos from field visits. The field belongs to soil reflectance group 6. Points represent the original unmixing results, lines show a smoothed trend.*

Fig. 10 shows a field belonging to soil reflectance group 3 cultivated with winter wheat in 2023, followed by a bare fallow period after harvest and during the following winter. At the beginning of June, the models predicted nearly full PV cover, with little to no soil or NPV presence. This was followed by a rapid decrease in PV in favor of NPV, as observed in image A from mid-July, where the wheat had reached full yellow ripeness. Harvesting occurred in August, resulting in a state of stubble fallow as shown in image B, with around 70% NPV, 30% soil, and nearly zero PV share estimated.

By the end of August, initial tillage practices were conducted, leading to higher estimated soil shares afterward (image C). Starting in September, very sparse spontaneous vegetation appeared on the field, as can be observed in image D. The spontaneous vegetation showed only little growth between October and February (images E to H). During this period, the PV share rose gently, while NPV and soil remained relatively stable at around 0.5, yet fluctuated during this period.

From February onwards, soil share began to rise rapidly, corresponding to the absence of visible green vegetation in images I to L, and a decreasing amount of NPV, particularly from images J to K, where tillage was visible. By mid-May, estimated soil cover was above 0.8, while NPV estimations were around 0.2, even though no NPV was observable in images K and L, which suggests an overestimation. Differences between the global and soil-specific predictions were less pronounced compared to Fig. 9 and no notable pattern was visible. Only during January 2024, global predictions rank soil over NPV while the opposite is the case for the soil-specific predictions.

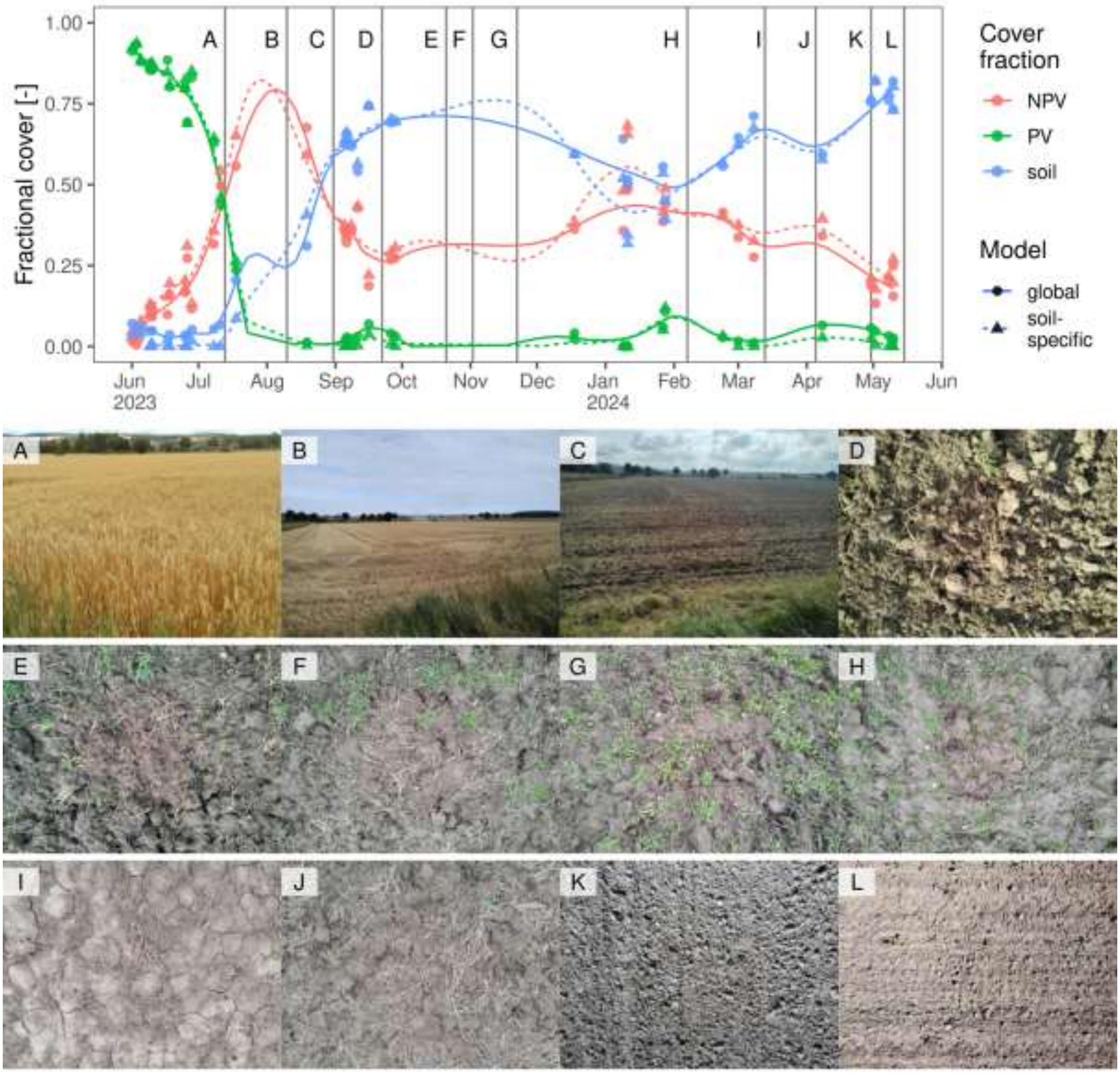


*Figure 10. Predicted fractional cover time series for photosynthetic vegetation (PV), non-photosynthetic vegetation (NPV), and soil for a field initially cultivated with winter wheat in 2023, followed by a bare soil period during winter and the seeding of a summer crop in spring, supplemented with photos from field visits. The field belongs to soil reflectance group 3. Points represent the original unmixing results, lines show a smoothed trend.*

## 5. Discussion

### *5.1. Fractional cover estimates*

We developed and evaluated an approach for predicting the fractional cover of NPV, PV, and soil across German croplands over time. Building on the methodology developed by Kowalski et al. (2023) and Okujeni et al. (2024) for grassland monitoring, we adapted the approach of regression-based unmixing to croplands and incorporated a novel extension that accounts for the impact of soil properties in predicting fractional cover. Overall, quantitative validation against multi-year reference data derived from VHR aerial imagery demonstrated the model's successful transferability from grassland monitoring to cropland applications. We found agreements for all cover fractions between the cropland reference data and the fractional covers from our model predictions.

While we found the same ranking for the accuracy of the three fractions, the absolute values differed slightly from the results of other studies on grassland. Okujeni et al. (2024) reported MAEs of 0.149, 0.067, and 0.135, for NPV, PV, and soil, respectively. Kowalski et al. (2023) also reported lower values with 0.137, 0.065, and 0.122. Compared to grasslands, arable land is subject to a greater variability of fractional cover due to different management and growth patterns within and between crop types. Consequently, a reduced accuracy for our PV and NPV fractional cover predictions compared to grasslands was anticipated. In Germany, plowing and tillage are regular practices in cropland cultivation, whereas such management practices are highly restricted on permanent grasslands. Extended periods without PV cover, dominated by mixtures of NPV and soil, as well as prolonged slow emergence of PV after sowing, are common on arable land and characterize the phenological cycle of most crops and all practices related to crop residue management. In general, grasslands only experience such states during droughts and mowing. This led to our samples covering the whole gradient of fraction mixtures, while the reference samples for the soil fraction on grasslands used by Okujeni et al. (2024) were concentrated around 0 to 0.2 and 0.8 to 1.

NPV and soil both exhibited lower performance than PV, indicating confusion between these cover fractions. This phenomenon has been noted in several studies on spectral unmixing and can be attributed to the high similarities in the spectral signatures of NPV and soil, which differ primarily in the SWIR region (Delegido et al., 2015). Similar results were also reported by Li et al. (2016) for open woodlands and grasslands in Northern China using multispectral GF-1 wide-field view data. They explained that certain combinations of bare soil and NPV result in ambiguous spectral signatures that are difficult to resolve, a limitation also highlighted by Okin et al. (2001) in their seminal study on the practical limits of hyperspectral vegetation discrimination. This issue aggravates when the intra-class variability within the spectral library is high, e.g., when multiple soil types are involved. Then, mixtures of dark soils with a small proportion of the generally brighter NPV cover may be misidentified as pure bright soils.

Our results also revealed that, for the same fraction, some value ranges were underestimated while others were overestimated, a pattern observed in other studies as well. Guerschman et al. (2015) noted similar findings, with low NPV and soil shares being overestimated, while higher shares tended to be underestimated. This trend was also observed by Dennison et al. (2019) in their study on cropland unmixing using simulated hyperspectral data. This might be due to the visually interpreted reference fractions. Although being commonly used to validate PV, NPV, and soil fractions when in-situ field data is unavailable, this method introduces uncertainty in labeling, as NPV and soil are not always clearly distinguishable in VHR imagery and it can be difficult to differentiate between pure and almost pure pixels.

### *5.2. Soil-Specific Unmixing*

The derivation of a soil reflectance composite for Germany provided the foundation for implementing the soil-specific unmixing approach, including both the development of the spectral library and the predictions of soil-specific cropland cover. This approach allows us to extract soil endmembers that represent the variability of soils across the study site, which is particularly valuable when no soil spectral database is available. Here, we even preferred this strategy over soil databases or official soil maps, because it supports not only developing soil-specific models but also soil-specific predictions, by determining the best-fitting model for each pixel based on the soil group map. The high spatial resolution of the soil reflectance composite of 30 m further enabled us to account for spectral soil differences even within a single field - something that official maps usually cannot achieve due to their lower resolution. Additionally, the soil reflectance composite provides the actual spectral signature of the pixel. This directly targets the challenge of determining the appropriate endmember for each pixel, especially for soil, as concluded by Li et al. (2016). Using this information addresses the problem of ambiguities in the unmixing of cropland with different soils.

The spectral signatures of the soil reflectance groups showed a high variability. The brightness gradient, especially in the visible spectrum, could indicate a general gradient of organic carbon content in the soil, with more organic carbon content absorbing more visible radiation (Udelhoven et al., 2003). Iron oxides were found to be related to the red and NIR parts of the spectrum (Chabrillat et al., 2019; Richter et al., 2009), where we also found a gradient between the spectra (Fig. 3). Another interesting finding was a less negative slope between SWIR1 and SWIR2 for soil group 3 compared to group 2, although being nearly identical in the visible and NIR. This could indicate that group 3 has a lower clay content, which is known to absorb especially in the SWIR2 region (Chabrillat et al., 2019).

The utilization of soil-specific models resulted in improvements in the NPV and soil fractional cover predictions. PV showed little to no changes attributed to this model change. For NPV, the overestimation was reduced while for soil we observed a reduced underestimation. This indicates that the soil-specific model was able to reduce the often-described uncertainties between NPV and soil depending on soil brightness, organic carbon content, and decomposition status of the NPV/organic matter (Verrelst et al., 2023). It is important to note that the improvements in soil accuracy did not come at the expense of NPV, and vice versa. At the same time, this method extension did not harm the PV predictions.

Laamrani et al. (2020) used Landsat 8 and linear spectral unmixing to estimate cropland soil cover in Canada, finding no significant improvement when accounting for soil types. They attributed this to their sampling being conducted in winter, when the soil was uniformly very wet and close to field capacity, making the differences between soil types less pronounced. Our year-round sampling may explain why we could not confirm their findings.

Training a model with all soil spectra combined reduces the number of bands with significant reflection differences between soil and NPV, due to the wide variation in soil reflection values. As can be taken from Fig. 3, when all soil spectra are considered at the same time, the primary differences from NPV are concentrated in the SWIR2 region and the slope between SWIR1 and SWIR2, which weakens the overall decision-making basis for the SVR models. In contrast, using a stratified model that includes only the soil spectra relevant to the pixel of interest excludes obsolete spectra, thereby strengthening the model's decision basis and improving accuracy. For example, soil group 1, despite being visually distinguishable from NPV spectra, exhibited the highest MAE when using the global model, possibly due to the global model's focus on the SWIR region. However, with the soil-specific model, we observed remarkable improvements in MAE for soil group 1, possibly because the model considered more bands when irrelevant soil spectra were excluded during training. This does not support the findings from other studies observing global models to be similar or even superior compared to models stratified by geographical regions or timeframes (Dudley et al., 2015; Kowalski et al., 2023). The differences between those and our findings could be attributed to several key differences in focus and methodology. First, unlike our study, which concentrated on croplands, both studies focused either on deriving fractional cover times in grasslands or the species-unmixing in forests and rangelands, presenting environments that are difficult to compare.

Additionally, while we stratified our models solely based on soil types, we used a global library comprising PV and NPV spectra for all crop types and multiple years across Germany. This could indicate a combination of the strengths coming from both stratification and generalization in our approach, leading to more accurate estimates.

Although the soil groups had varying sample sizes and distributions, potentially limiting the robustness of estimates and conclusions about the relationship between spectral features and soil-specific unmixing performance, our results showed overall improvement across all soil types. The scatterplots per soil type reinforced this (Fig. 6), neither revealing a major decrease in performance for any soil group nor indicating that only specific groups benefited from the soil-specific approach. This consistency underscores the effectiveness of our method.

### *5.3. Monitoring of Cropland with Fractional Cover Time Series*

The available field photos provided a unique data source for qualitative validation and were valuable for comparing time series fractional cover estimates to observed vegetation dynamics and management events on the field. They also helped assess the suitability of the time series for real-world monitoring tasks beyond single measurement comparisons. For the two winter wheat fields, we observed very similar trajectories of the fractional cover estimates from the beginning of our observation period until harvest, indicating consistency between the same crop types. Remarkable differences, however, were observed during winter. Depending on whether the field was left as bare fallow during winter or a cover crop was cultivated and removed in spring before sowing a new spring crop, we found distinct patterns in the time series that accurately reflected the field cover changes during these measures, even if only minor field activities, such as spontaneous greening, are visible in the PV time series.

Some time series did not reach 0 or 1 despite observing full PV cover or bare soil in the field photos. This indicates that the overall uncertainties observed in the quantitative evaluation are also present in the specific time series for our test fields. NPV sometimes only reached low values when PV was the dominant cover fraction (Fig. 10), while soil dominance often led to NPV being overestimated. This finding highlights that there is still some confusion remaining between these two classes, though no confusion was noted between NPV and PV. Despite these uncertainties in estimating exact cover fractions, the method has proven well-suited for capturing the dominant cover type and its temporal development.

Germany also experienced a very cloudy and rainy autumn and winter in 2023/24. This is reflected in a low density of cloud-free observations that we observed in the satellite data time series. Since winter is among the most important periods for soil cover monitoring, this might be a potential shortcoming of the datasets. However, we have also seen that even under these unfavorable weather conditions, specific management practices like cover crops and bare fallow periods could be traced in our time series.

## 6. Conclusion

Our study confirms the effectiveness of spectral unmixing using Sentinel-2 and Landsat data for cropland monitoring. The method delivers reliable time series of NPV, PV, and soil fractional cover, offering valuable insights for continuous monitoring of cropland management, agricultural carbon cycle assessments, and soil erosion modeling. By integrating Landsat data, our approach enables multidecadal monitoring, extending the analysis back before the Sentinel era.

A key advancement in our research is the introduction of a soil-specific unmixing approach, which enhances the accuracy of fractional cover estimates by selecting the most appropriate model based on the soil spectral signature of each pixel. This method proved particularly effective across diverse soil types, as demonstrated in our multi-year, Germany-wide validation. The reliance on free and open remote sensing data, rather than official soil maps, makes this approach transferable to other regions. The qualitative evaluation of fractional cover time series, supported by repeated field cover photos, underscored the practical applications of these time series and highlighted crucial information needs that can be derived from it.

Looking ahead, future research should explore the potential of hyperspectral time series to further refine these estimates. Additionally, future field campaigns should consider data collection at identical points with constant acquisition geometries to enable highly accurate derivation of cover fractions from the images. This study lays the groundwork for applying our method to large-scale assessments of cropland cover, providing an essential database for modeling carbon emissions and sequestration related to agricultural land use at the national level and beyond.

## Author contributions

**Felix Lobert:** Conceptualization, Methodology, Software, Validation, Formal analysis, Investigation, Visualization, Writing - Original Draft, Writing - Review & Editing. **Marcel Schwieder:** Conceptualization, Methodology, Investigation, Writing - Review & Editing. **Jonas Alsleben:** Methodology, Software, Writing - Review & Editing. **Tom Brög:** Methodology, Writing - Review & Editing. **Katja Kowalski:** Conceptualization, Methodology, Software, Writing - Review & Editing. **Akpona Okujeni:** Conceptualization, Methodology, Software, Writing - Review & Editing. **Patrick Hostert:** Conceptualization, Supervision, Writing - Review & Editing. **Stefan Erasmi:** Conceptualization, Supervision, Writing - Review & Editing

**Declaration of generative AI and AI-assisted technologies in the writing process**

During the preparation of this work, the authors used ChatGPT to improve the readability and language of the manuscript. After using this tool, the authors reviewed and edited the content as needed and take full responsibility for the content of the published article.

## References


Adams, J.B., Smith, M.O., Johnson, P.E., 1986. Spectral mixture modeling: A new analysis of rock and soil types at the Viking Lander 1 Site. Journal of Geophysical Research: Solid Earth 91, 8098–8112. https://doi.org/10.1029/JB091iB08p08098

Atkinson, P.M., Cutler, M.E.J., Lewis, H., 1997. Mapping sub-pixel proportional land cover with AVHRR imagery. International Journal of Remote Sensing 18, 917–935. https://doi.org/10.1080/014311697218836

Barnes, M.L., Yoder, L., Khodaee, M., 2021. Detecting Winter Cover Crops and Crop Residues in the Midwest US Using Machine Learning Classification of Thermal and Optical Imagery. Remote Sensing 13, 1998. https://doi.org/10.3390/rs13101998

Blickensdörfer, L., Schwieder, M., Pflugmacher, D., Nendel, C., Erasmi, S., Hostert, P., 2022. Mapping of crop types and crop sequences with combined time series of Sentinel-1, Sentinel-2 and Landsat 8 data for Germany. Remote Sensing of Environment 269. https://doi.org/10.1016/j.rse.2021.112831

Bolton, D.K., Gray, J.M., Melaas, E.K., Moon, M., Eklundh, L., Friedl, M.A., 2020. Continental-scale land surface phenology from harmonized Landsat 8 and Sentinel-2 imagery. Remote Sensing of Environment 240, 111685. https://doi.org/10.1016/j.rse.2020.111685

Bouroubi, Y., Tremblay, N., Vigneault, P., Benoit, M., 2014. Linear spectral unmixing for crop and soil information extraction from a single worldview-2 image, in: 2014 IEEE Geoscience and Remote Sensing Symposium. Presented at the 2014 IEEE Geoscience and Remote Sensing Symposium, pp. 5103–5106. https://doi.org/10.1109/IGARSS.2014.6947645

Broeg, T., Don, A., Gocht, A., Scholten, T., Taghizadeh-Mehrjardi, R., Erasmi, S., 2024. Using local ensemble models and Landsat bare soil composites for large-scale soil organic carbon maps in cropland. Geoderma 444, 116850. https://doi.org/10.1016/j.geoderma.2024.116850

Carpenter, G.A., Gopal, S., Macomber, S., Martens, S., Woodcock, C.E., 1999. A Neural Network Method for

Mixture Estimation for Vegetation Mapping. Remote Sensing of Environment 70, 138–152. https://doi.org/10.1016/S0034-4257(99)00027-9

Chabrillat, S., Ben-Dor, E., Cierniewski, J., Gomez, C., Schmid, T., Van Wesemael, B., 2019. Imaging Spectroscopy for Soil Mapping and Monitoring. Surv Geophys 40, 361–399. https://doi.org/10.1007/s10712-019-09524-0

Coulibaly, L.K., Guan, Q., Assoma, T.V., Fan, X., Coulibaly, N., 2021. Coupling linear spectral unmixing and RUSLE2 to model soil erosion in the Boubo coastal watershed, Côte d'Ivoire. Ecological Indicators 130, 108092. https://doi.org/10.1016/j.ecolind.2021.108092

Delegido, J., Verrelst, J., Rivera, J.P., Ruiz-Verdú, A., Moreno, J., 2015. Brown and green LAI mapping through spectral indices. International Journal of Applied Earth Observation and Geoinformation 35, 350–358. https://doi.org/10.1016/j.jag.2014.10.001

Demattê, J.A.M., Fongaro, C.T., Rizzo, R., Safanelli, J.L., 2018. Geospatial Soil Sensing System (GEOS3): A powerful data mining procedure to retrieve soil spectral reflectance from satellite images. Remote Sensing of Environment 212, 161–175. https://doi.org/10.1016/j.rse.2018.04.047

Dennison, P.E., Qi, Y., Meerdink, S.K., Kokaly, R.F., Thompson, D.R., Daughtry, C.S.T., Quemada, M., Roberts, D.A., Gader, P.D., Wetherley, E.B., Numata, I., Roth, K.L., 2019. Comparison of Methods for Modeling Fractional Cover Using Simulated Satellite Hyperspectral Imager Spectra. Remote Sensing 11, 2072. https://doi.org/10.3390/rs11182072

Deutscher Wetterdienst, 2024. German Climate Atlas [WWW Document]. URL https://www.dwd.de/EN/climate_environment/climateatlas/climateatlas_node.html (accessed 7.31.24).

Dudley, K.L., Dennison, P.E., Roth, K.L., Roberts, D.A., Coates, A.R., 2015. A multi-temporal spectral library approach for mapping vegetation species across spatial and temporal phenological gradients. Remote Sensing of Environment, Special Issue on the Hyperspectral Infrared Imager (HyspIRI) 167, 121–134. https://doi.org/10.1016/j.rse.2015.05.004

Dudley, N., Alexander, S., 2017. Agriculture and biodiversity: a review. Biodiversity 18, 45–49. https://doi.org/10.1080/14888386.2017.1351892

Dvorakova, K., Heiden, U., Pepers, K., Staats, G., van Os, G., van Wesemael, B., 2023. Improving soil organic carbon predictions from a Sentinel–2 soil composite by assessing surface conditions and uncertainties. Geoderma 429, 116128. https://doi.org/10.1016/j.geoderma.2022.116128

Eurostat, 2024. Land cover statistics [WWW Document]. URL https://ec.europa.eu/eurostat/statistics-

explained/index.php?title=Land_cover_statistics (accessed 4.23.24).
Federal Statistical Office, 2024. Field crops and grassland [WWW Document]. Federal Statistical Office. URL https://www.destatis.de/EN/Themes/Economic-Sectors-Enterprises/Agriculture-Forestry-Fisheries/Field-Crops-Grassland/_node.html (accessed 7.31.24).
Frantz, D., 2019. FORCE-Landsat + Sentinel-2 analysis ready data and beyond. Remote Sensing 11. https://doi.org/10.3390/rs11091124
Guerschman, J.P., Hill, M.J., Leys, J., Heidenreich, S., 2020. Vegetation cover dependence on accumulated antecedent precipitation in Australia: Relationships with photosynthetic and non-photosynthetic vegetation fractions. Remote Sensing of Environment 240, 111670. https://doi.org/10.1016/j.rse.2020.111670
Guerschman, J.P., Hill, M.J., Renzullo, L.J., Barrett, D.J., Marks, A.S., Botha, E.J., 2009. Estimating fractional cover of photosynthetic vegetation, non-photosynthetic vegetation and bare soil in the Australian tropical savanna region upscaling the EO-1 Hyperion and MODIS sensors. Remote Sensing of Environment 113, 928–945. https://doi.org/10.1016/j.rse.2009.01.006
Guerschman, J.P., Scarth, P.F., McVicar, T.R., Renzullo, L.J., Malthus, T.J., Stewart, J.B., Rickards, J.E., Trevithick, R., 2015. Assessing the effects of site heterogeneity and soil properties when unmixing photosynthetic vegetation, non-photosynthetic vegetation and bare soil fractions from Landsat and MODIS data. Remote Sensing of Environment 161, 12–26. https://doi.org/10.1016/j.rse.2015.01.021
Johnson, J.M.F., Franzluebbers, A.J., Weyers, S.L., Reicosky, D.C., 2007. Agricultural opportunities to mitigate greenhouse gas emissions. Environmental Pollution 150, 107–124. https://doi.org/10.1016/j.envpol.2007.06.030
Kowalski, K., Okujeni, A., Brell, M., Hostert, P., 2022. Quantifying drought effects in Central European grasslands through regression-based unmixing of intra-annual Sentinel-2 time series. Remote Sensing of Environment 268, 112781. https://doi.org/10.1016/j.rse.2021.112781
Kowalski, K., Okujeni, A., Hostert, P., 2023. A generalized framework for drought monitoring across Central European grassland gradients with Sentinel-2 time series. Remote Sensing of Environment 286, 113449. https://doi.org/10.1016/j.rse.2022.113449
Kross, A., Kaur, G., Jaeger, J.A.G., 2022. A geospatial framework for the assessment and monitoring of environmental impacts of agriculture. Environmental Impact Assessment Review 97, 106851–106851. https://doi.org/10.1016/j.eiar.2022.106851

Laamrani, A., Joosse, P., McNairn, H., Berg, A.A., Hagerman, J., Powell, K., Berry, M., 2020. Assessing Soil Cover Levels during the Non-Growing Season Using Multitemporal Satellite Imagery and Spectral Unmixing Techniques. Remote Sensing 12, 1397. https://doi.org/10.3390/rs12091397

Lal, R., 2009. Challenges and opportunities in soil organic matter research. European Journal of Soil Science 60, 158–169. https://doi.org/10.1111/j.1365-2389.2008.01114.x

Lewińska, K.E., Frantz, D., Leser, U., Hostert, P., 2024. Usable observations over Europe: evaluation of compositing windows for Landsat and Sentinel-2 time series. European Journal of Remote Sensing 57, 2372855. https://doi.org/10.1080/22797254.2024.2372855

Lewińska, K.E., Hostert, P., Buchner, J., Bleyhl, B., Radeloff, V.C., 2020. Short-term vegetation loss versus decadal degradation of grasslands in the Caucasus based on Cumulative Endmember Fractions. Remote Sensing of Environment 248, 111969. https://doi.org/10.1016/j.rse.2020.111969

Li, X., Zheng, G., Wang, J., Ji, C., Sun, B., Gao, Z., 2016. Comparison of Methods for Estimating Fractional Cover of Photosynthetic and Non-Photosynthetic Vegetation in the Otindag Sandy Land Using GF-1 Wide-Field View Data. Remote Sensing 8, 800. https://doi.org/10.3390/rs8100800

Lloyd, S., 1982. Least squares quantization in PCM. IEEE Transactions on Information Theory 28, 129–137. https://doi.org/10.1109/TIT.1982.1056489

Lobert, F., Löw, J., Schwieder, M., Gocht, A., Schlund, M., Hostert, P., Erasmi, S., 2023. A deep learning approach for deriving winter wheat phenology from optical and SAR time series at field level. Remote Sensing of Environment 298, 113800. https://doi.org/10.1016/j.rse.2023.113800

McClelland, S.C., Paustian, K., Schipanski, M.E., 2021. Management of cover crops in temperate climates influences soil organic carbon stocks: a meta-analysis. Ecological Applications 31, 1–19. https://doi.org/10.1002/eap.2278

Meusburger, K., Konz, N., Schaub, M., Alewell, C., 2010. Soil erosion modelled with USLE and PESERA using QuickBird derived vegetation parameters in an alpine catchment. International Journal of Applied Earth Observation and Geoinformation 12, 208–215. https://doi.org/10.1016/j.jag.2010.02.004

Mzid, N., Pignatti, S., Huang, W., Casa, R., 2021. An Analysis of Bare Soil Occurrence in Arable Croplands for Remote Sensing Topsoil Applications. Remote Sensing 13, 474. https://doi.org/10.3390/rs13030474

Okin, G.S., Roberts, D.A., Murray, B., Okin, W.J., 2001. Practical limits on hyperspectral vegetation discrimination in arid and semiarid environments. Remote Sensing of Environment 77, 212–225. https://doi.org/10.1016/S0034-4257(01)00207-3

Okujeni, A., Kowalski, K., Lewińska, K.E., Schneidereit, S., Hostert, P., 2024. Multidecadal grassland fractional cover time series retrieval for Germany from the Landsat and Sentinel-2 archives. Remote Sensing of Environment 302, 113980. https://doi.org/10.1016/j.rse.2023.113980

Okujeni, A., Van Der Linden, S., Tits, L., Somers, B., Hostert, P., 2013. Support vector regression and synthetically mixed training data for quantifying urban land cover. Remote Sensing of Environment 137, 184–197. https://doi.org/10.1016/j.rse.2013.06.007

Öttl, L.K., Wilken, F., Juřicová, A., Batista, P.V.G., Fiener, P., 2024. A millennium of arable land use – the long-term impact of tillage and water erosion on landscape-scale carbon dynamics. SOIL 10, 281–305. https://doi.org/10.5194/soil-10-281-2024

Pacheco, A., McNairn, H., 2010. Evaluating multispectral remote sensing and spectral unmixing analysis for crop residue mapping. Remote Sensing of Environment 114, 2219–2228. https://doi.org/10.1016/j.rse.2010.04.024

Pham, V.-D., Tetteh, G., Thiel, F., Erasmi, S., Schwieder, M., Frantz, D., Van Der Linden, S., 2024. Temporally transferable crop mapping with temporal encoding and deep learning augmentations. International Journal of Applied Earth Observation and Geoinformation 129, 103867. https://doi.org/10.1016/j.jag.2024.103867

Poeplau, C., Don, A., 2015. Carbon sequestration in agricultural soils via cultivation of cover crops – A meta-analysis. Agriculture, Ecosystems & Environment 200, 33–41. https://doi.org/10.1016/j.agee.2014.10.024

Richter, N., Jarmer, T., Chabrillat, S., Oyonarte, C., Hostert, P., Kaufmann, H., 2009. Free Iron Oxide Determination in Mediterranean Soils using Diffuse Reflectance Spectroscopy. Soil Science Soc of Amer J 73, 72–81. https://doi.org/10.2136/sssaj2008.0025

Roberts, D.A., Gardner, M., Church, R., Ustin, S., Scheer, G., Green, R.O., 1998. Mapping Chaparral in the Santa Monica Mountains Using Multiple Endmember Spectral Mixture Models. Remote Sensing of Environment 65, 267–279. https://doi.org/10.1016/S0034-4257(98)00037-6

Schulz, C., Holtgrave, A., Kleinschmit, B., 2021. Large-scale winter catch crop monitoring with Sentinel-2 time series and machine learning – An alternative to on-site controls? Computers and Electronics in Agriculture 186, 106173. https://doi.org/10.1016/j.compag.2021.106173

Schwieder, M., Tetteh, G.O., Blickensdörfer, L., Gocht, A., Erasmi, S., 2024. Agricultural land use (raster) : National-scale crop type maps for Germany from combined time series of Sentinel-1, Sentinel-2 and

Landsat data (2017 to 2021). https://doi.org/10.5281/zenodo.10640528

Seitz, D., Fischer, L.M., Dechow, R., Wiesmeier, M., Don, A., 2023. The potential of cover crops to increase soil organic carbon storage in German croplands. Plant Soil 488, 157–173. https://doi.org/10.1007/s11104-022-05438-w

Shimabukuro, Y.E., Smith, J.A., 1991. The least-squares mixing models to generate fraction images derived from remote sensing multispectral data. IEEE Transactions on Geoscience and Remote Sensing 29, 16–20. https://doi.org/10.1109/36.103288

Tetteh, G.O., Schwieder, M., Erasmi, S., Conrad, C., Gocht, A., 2023. Comparison of an Optimised Multiresolution Segmentation Approach with Deep Neural Networks for Delineating Agricultural Fields from Sentinel-2 Images. PFG 91, 295–312. https://doi.org/10.1007/s41064-023-00247-x

Tscharntke, T., Clough, Y., Wanger, T.C., Jackson, L., Motzke, I., Perfecto, I., Vandermeer, J., Whitbread, A., 2012. Global food security, biodiversity conservation and the future of agricultural intensification. Biological Conservation, ADVANCING ENVIRONMENTAL CONSERVATION: ESSAYS IN HONOR OF NAVJOT SODHI 151, 53–59. https://doi.org/10.1016/j.biocon.2012.01.068

Tucker, C.J., 1979. Red and photographic infrared linear combinations for monitoring vegetation. Remote Sensing of Environment 8, 127–150. https://doi.org/10.1016/0034-4257(79)90013-0

Udelhoven, T., Emmerling, C., Jarmer, T., 2003. Quantitative analysis of soil chemical properties with diffuse reflectance spectrometry and partial least-square regression: A feasibility study. Plant and Soil 251, 319–329. https://doi.org/10.1023/A:1023008322682

Van der Linden, S., Rabe, A., Held, M., Jakimow, B., Leitão, P.J., Okujeni, A., Schwieder, M., Suess, S., Hostert, P., 2015. The EnMAP-Box—A Toolbox and Application Programming Interface for EnMAP Data Processing. Remote Sensing 7, 11249–11266. https://doi.org/10.3390/rs70911249

Van Deventer, A.P., Ward, A.D., Gowda, P.M., Lyon, J.G., 1997. Using thematic mapper data to identify contrasting soil plains and tillage practices. Photogrammetric Engineering and Remote Sensing 63, 87–93.

Verrelst, J., Halabuk, A., Atzberger, C., Hank, T., Steinhauser, S., Berger, K., 2023. A comprehensive survey on quantifying non-photosynthetic vegetation cover and biomass from imaging spectroscopy. Ecological Indicators 155, 110911. https://doi.org/10.1016/j.ecolind.2023.110911

Vrieling, A., 2006. Satellite remote sensing for water erosion assessment: A review. CATENA 65, 2–18. https://doi.org/10.1016/j.catena.2005.10.005

Yue, J., Qingjiu Tian, Tian, Q., Xinyu Dong, Dong, X., Nianxu Xu, Xu, N., 2020. Using broadband crop residue angle index to estimate the fractional cover of vegetation, crop residue, and bare soil in cropland systems. Remote Sensing of Environment 237, 111538. https://doi.org/10.1016/j.rse.2019.111538

Yue, J., Tian, Q., Tang, S., Kaijian Xu, Xu, K., Kaijian Xu, Chengquan Zhou, Zhou, C., 2019. A dynamic soil endmember spectrum selection approach for soil and crop residue linear spectral unmixing analysis. International Journal of Applied Earth Observation and Geoinformation 78, 306–317. https://doi.org/10.1016/j.jag.2019.02.001